A Numerical Study on the Drainage Characteristics of Geotextile in Unsaturated Fine-grained Soil

Amalesh Jana[1], Arindam Dey[2]

Abstract

Geotextile is widely utilized as a drainage medium in many geotechnical and transportation infrastructures, such as pavement design, earth retaining structures, embankments, and slope stability. Its successful implementation has been observed across numerous projects. Nevertheless, there have been questions over the efficacy of geotextile drainage in unsaturated soil due to its capillary barrier characteristics. This work conducts a numerical analysis to examine the hydraulic properties of geotextile and its effectiveness as a drainage system in unsaturated fine-grained soil. This study investigates the dual characteristics of geotextile (Capillary barrier and drainage) in an unsaturated soil environment by analyzing transient seepage. Initially, a numerical simulation is performed by calibrating a numerical model with the results acquired from laboratory infiltration testing. The investigation involved the simulation of geotextile drainage, considering both the horizontal and vertical directions, while also considering the presence or absence of vertical drainage. Furthermore, a comprehensive evaluation was undertaken to analyze the drainage characteristics of geotextile, considering different levels of moisture in the underlying soil and successive stages of infiltration, encompassing wetting and drying cycles. In order to highlight the importance of the air entry suction value of geotextiles as lateral drainage systems in unsaturated soil, numerical simulations utilize a total of seven various types of geotextiles. In summary, the numerical investigation provides valuable insights into the drainage behavior of geotextiles in

[1]Assistant Professor, Civil Engineering, Montana State University, Bozeman, MT 59717 (corresponding author), E-mail: amalesh.jana@montana.edu
[2]Associate Professor, Department of Civil Engineering, Indian Institute of Technology Guwahati, India, arindam.dey@iitg.ac.in

unsaturated soil environments. The findings from this study can inform designers in making informed decisions when designing drainage systems, taking into account the unsaturated properties of the geotextile material.

Keywords

Nonwoven geotextile; Capillary barrier; Infiltration; Unsaturated soil; Breakthrough suction; Drainage function; Marginal soil

1 Introduction

Geotextiles are essential components in road and pavement construction, specifically for facilitating effective drainage. They are strategically placed to prevent the mixing of different soil layers, while simultaneously enabling efficient water drainage. Geotextiles assist in managing excess water and preventing waterlogging, ensuring that water is properly channeled away from the pavement structure. This drainage function contributes to the overall stability, durability, and longevity of roads and pavements by reducing the potential for erosion, weakening, and deterioration caused by stagnant or poorly managed water. Besides, geotextile has been used in many geotechnical and geoenvironmental applications to provide multiple functions to the system such as reinforcement, separation, filtration, and drainage. There are mainly three types of geotextiles: woven, nonwoven, and wicking geotextiles, which are classified based on their manufacturing process. The highly permeable formation of nonwoven geotextile makes them efficient drainage medium which is used in pavement design, earth retaining structures and embankments when they are comprised with poorly draining soils (Tatsuoka and Yamauchi, 1986; Mitchell and Zornberg, 1995; Benjamin et al., 2007; Portelinha et al., 2013, 2014; Portelinha and Zornberg, 2017). However, use of fine-grained soils as the fill materials is not recommended in several design guidelines due to the poor performance during rainwater infiltration (AASHTO, 2014; NCMA, 2010). Internal and external water causes the unsatisfactory performance of the geosynthetic soil structures. However, application of locally available marginal soil (with low hydraulic conductivity) in geotechnical and transportation infrastructure is the very cost-effective and sustainable solution for infrastructure development (Christopher and Stuglis, 2005; Kim and Borden, 2013; Miyata and Bathurst, 2007; Esmaili et al., 2014). In this regard, many laboratory and field investigations reported about the drainage characteristics of nonwoven geotextile in the

presence of fine soil. Such provisions increase the stability of the fine-grained soil by draining out the infiltrated rainwater from the system. Bhattacherjee and Viswanadham (2015) performed seepage analysis of a silty sand slope reinforced by hybrid-geosynthetic layers and illustrated their efficacy in lowering the phreatic surface by dissipating excess pore water pressure due to rainfall infiltration.

In the field, soils are compacted lesser than their optimum moisture content and, hence, remain unsaturated (Thuo et al., 2015; Vahedifard et al., 2016). In unsaturated fine-grained soil medium, capillary barrier action of geotextile is reported in many studies which raises a concern about their effective performance as drainage layer under such cases (Iryo and Rowe, 2003, 2005; Bouazza et al., 2006; Bathurst and Ho, 2009; Zornberg et al., 2010; Bouazza et al., 2013; Thuo et al., 2015; Jana and Dey, 2016, 2017; Zornberg et al., 2017). When the overlying fine-grained soil is unsaturated, water cannot migrate to the geotextile layer due to the contrasting difference in their hydraulic conductivities. Water can migrate to the geotextile layer after attaining the breakthrough suction of the geotextile, wherein the hydraulic conductivity of soil and geotextile is the same (Zornberg et al., 2010). Portelinha and Zornberg (2017) performed full-scale seepage analysis of geotextile reinforced soil wall in a controlled rainwater infiltration. The full-scale test results indicated capillary break at the soil-geotextile interface resulting retardation of infiltration front. Several studies have acknowledged the beneficial impact of wicking geotextile in minimizing the capillary barrier effect in the lateral direction, as opposed to the cross-plane direction, by facilitating drainage in the lateral direction. Nevertheless, experts are currently conducting investigations into these provisions and numerical simulation of unsaturated flow characteristics are severely limited (Zornberg et al. 2017; Biswas et al. 2021; Lin et al. 2022).

The previous discussions explain the complex behavior of the geotextile in unsaturated soil medium. Despite the wealth of research, there are still several characteristics as observed in the experimental investigations which are needed to be scrutinized to develop a comprehensive understanding of the waterfront movement and pore-water pressure generation throughout the soil-geotextile system. It is very challenging to get complete information of the whole system using sensors inserted within the test model since the influence area of the sensor is decidedly less compared to the scale of the system. Sometimes it is challenging to perform full-scale field and laboratory infiltration test of marginal soil owing to an extremely time-consuming experiment accompanied by a complicated methodology. In such cases, a suitable calibrated numerical model can provide valuable information of the whole system before performing the full-scale and laboratory tests. The primary motive of the present study is to investigate the complex behavior of nonwoven geotextile as drainage material to provide a comprehensive understanding of water flow characteristics within an unsaturated soil medium. First, a numerical model of the unsaturated flow of water was simulated and verified with laboratory investigation. The in-plane drainage characteristics of various geotextiles were simulated under various boundary conditions to elucidate drainage mechanism of geotextile in unsaturated condition.

2 Numerical analysis of transient seepage flow in unsaturated soil medium

2.1 Calibration of numerical model

Transient seepage through the unsaturated soil-geotextile system was numerically simulated using a finite element program GeoStudio SEEP/W module. SEEP/W uses Richards (1931) equation to solve the nonlinear two-dimensional flow of water in the unsaturated soil. Bouazza et al. (2006, 2013) performed water flow in a soil column consisting of clay layer underlain by sand. The thickness of the top clay layer was 30 cm, underlain by a sand layer of thickness 15 cm (Fig.

1a). The diameter of the cylindrical soil column was 20 cm. Constant rate of water was supplied on the top of the soil column. Water flow through the soil was monitored by observing the change in volumetric water content of the soil with the lapsed time (Bouazza et al., 2006, 2013). In the current study, a numerical model of the soil column was developed which is presented in the Fig. 1b. Four-node quadrilateral element is used discretized the soil domain. The boundary conditions were characteristically chosen to simulate the one-dimensional flow of water through the soil column. An impermeable boundary was used at the lateral edge of the soil column to prevent any transverse flow of the water. An impermeable boundary was also provided at the base of the soil column allowing accumulation of seepage water (Fig. 1b). A constant rate of unit flux (5.72×10^{-8} mm/s) was provided at the topmost free boundary of the soil column to simulate rainwater infiltration. During infiltration, the surface runoff from the model was ensured upon the generation of positive pore water pressure at the topmost boundary. Such runoff was numerically achieved by updating the boundary condition from the constant unit flux boundary to a zero pore-pressure boundary, thus ensuring no ponding of water on the top surface of the numerical model. This method confirmed the practical one-dimensional soil column model for rainwater infiltration test.

In this study, Van Genuchten (1980) model (Eq. 1-3) has been used to define the unsaturated hydraulic properties of the geotextile and soil. The model-fitting parameters as adopted are shown in Table 1. The water retention and corresponding hydraulic conductivity curves are presented in Fig. 2.

$$\theta_w = \theta_r + \frac{\theta_s - \theta_r}{[1+(\alpha\psi)^n]^m} \tag{1}$$

$$k_w = k_s \frac{[1-(\alpha\psi)^{(n-1)}\{1+(\alpha\psi)^n\}^{-m}]^2}{[1+(\alpha\psi)^n]^{m/2}} \tag{2}$$

$$n = \frac{1}{1-m} \tag{3}$$

where, θ_w represents the volumetric water content, θ_r indicates the residual water content, θ_s denotes the saturated water content, ψ is the suction, k_w is the hydraulic conductivity at a particular suction value, k_s is the saturated hydraulic conductivity, α, n and m are the model fitting parameters. The initial unsaturated state of the soil was defined by the moisture content of the soil which governs the transient flow of water through the soil medium. In the numerical simulation, the initial volumetric moisture content of sand and clay was considered 5% and 12% as reported in the laboratory investigation (Bouazza et al., 2006, 2013).

2.2 Methodology

Richard's equation was used to mathematically model the transient unsaturated flow of water which is given as

$$k_x \frac{\partial^2 h}{\partial x^2} + k_y \frac{\partial^2 h}{\partial y^2} = \frac{\partial \theta_w}{\partial t} = m_w \gamma_w \frac{\partial h}{\partial t} \tag{4}$$

where, k_x and k_y denote the unsaturated hydraulic conductivities at a given suction, h represents the total head, θ_w is the volumetric moisture content and, m_w indicates the slope of the storage curve. SEEP/W is a finite element program which numerically solves seepage analysis based on Darcy's Law, for which the corresponding finite element transient seepage equation can be written as

$$[k]\{H\} + [M]\{H\}, t = \{Q\} \tag{5}$$

where, $[k]$ is the unsaturated conductivity matrix at a given suction, $\{H\}$ represents the total head vector at the nodes, $\{Q\}$ is the flux vector at the corresponding nodes, and $[M]$ denotes element mass matrix. In transient seepage analysis, at any time step, the total head at each node is

numerically solved from the defined and estimated total head (previous time step), while utilizing the unit flux defined at the boundary nodes.

2.3 Calibration Results

The pore water pressure distribution throughout the soil column is shown in Fig. 3a. The one-dimensional flow of water through the soil column is assured as there is no flow along the side and bottom boundary of the model, indicated by zero flux at the edges as represented in Fig. 3a. After performing transient seepage analysis, the volumetric water content at four specific nodes within the soil column (A, B, C, and D) was monitored for the entire duration of seepage. These nodes were chosen as per the location of pore-pressure measurement sensors in the experiment by Bouazza et al. (2006). The change in volumetric water content at these specific locations as reported in Bouazza et al. (2006, 2013) is presented in Fig. 3b. The corresponding variation of water content at these four nodes obtained from the numerical simulation is shown in Fig. 4a. Fig. 3b and Fig 4a indicate that the numerical results sufficiently resemble the laboratory experiment result. The volumetric water content of Node A gradually increased with time from its initial value of 12%. A similar trend was observed for the other nodes. The time taken to reach the infiltrated water at a different node in the soil column is matched with the results from laboratory experiment. The laboratory experiment results showed marginally lesser volumetric water content at different nodes compared to numerical simulation results. This is attributed to the air entrapment in the soil pores in the physical model (Iryo and Rowe, 2004), which was not considered in the finite element simulations. The pore pressure generated at these nodes at different instant of time is shown in Fig. 4b. The suction of the soil decreased gradually from its initial value during rainwater infiltration, thereby indicating progressive saturation of the soil column. Regardless the effect of possible air entrapment, the developed numerical simulation effectively predicted the unsaturated flow of

water in a soil medium during rainwater infiltration which ascertained the suitability of numerical model to investigate unsaturated seepage flow. Following successful calibration of numerical model, similar methodology is implemented to simulate drainage characteristics of geotextile as described below.

3 Drainage behavior of geotextile in the one-dimensional soil column under different soil and boundary condition

In this section, a stepwise procedure was implemented to investigate the response of geotextile as a drainage material in saturated and unsaturated conditions. This section consists of five different cases of seepage analysis through a clay soil column. The primary aim was to eloquently delineate the drainage response of the geotextile for straightforward and easy understanding of its drainage mechanism.

3.1 Water flow in one-dimensional soil column in the absence of geotextile

A numerical model of the soil column was developed to monitor the infiltration of water through the clay column. The boundary conditions and hydraulic characteristics of the model were similar to the previous analysis. The sand layer was replaced by identical overlying clay soil (Fig. 5a). The initial moisture content of the clay was assumed 18%. A constant rate of infiltration (unit flux 5.72×10^{-8} mm/s) was applied on the top of the soil column. After 200 h of infiltration, the pore pressure distribution within the soil column is shown in Fig. 6b. It can be stated that the pore water pressure contours obtained from the transient seepage analysis imitates the fully submergence condition of the soil column. Since the entire soil column reached fully saturated state at the end of 200 h infiltration, the variation of pore water pressure along the height is equivalent to the pore water pressure under submergence condition. Variation of moisture content at three nodes (Node 1, 2, and 3 in Fig 6a) was examined and presented in Fig. 7a, demonstrating a gradual saturation of soil as waterfront progressed through the soil column during infiltration.

3.2 Water flow in the soil column in the presence of geotextile

In this section, a geotextile of 3 mm thickness was inserted inside the clay at an elevation 15 cm as shown in the Fig. 5b. However, geotextile was not inserted inside the vertical drain to prevent any lateral flow through the geotextile. Only the flow in the cross-plane direction (i.e. towards the bottom of the soil model) was investigated. A discontinuity of impermeable boundary between the drain and the geotextile can be seen in Fig. 5b. The water characteristics curve of the geotextile is presented in Fig. 2. In case of geotextile, the water entry suction is approximately 1 kPa, which is a relatively lower value compared to that of the fine clay soil. If the suction of the unsaturated soil is more than the water entry suction of the geotextile, geotextile remains impermeable because at any given suction, the conductivity of the geotextile is decidedly lower than the fine clay. The boundary condition and hydraulic properties of the soil were identical as adopted in the previous analysis. After performing transient seepage analysis, the waterfront migration in the clay column was monitored in the presence of geotextile. The pore water pressure distribution inside the soil column at 200 h is shown in Fig. 6b. It can be observed that the geotextile acts as barrier material by preventing water migration into the soil layer beneath it. The soil above the geotextile reaches its saturation point whereas the soil beneath the geotextile is in unsaturated condition. The change in the moisture content of the soil at different time instances is shown in Fig. 7b. It can be observed that Node 1 and Node 2 reaches the saturation point, whereas there is no change of water content at Node 3, thereby indicating barrier action of geotextile. It can be observed from Fig. 7a that without the geotextile layer, there was a change in water content at Node 3. On the other hand, for the same Node 3, due to the presence of geotextile, there has been insignificant change in water content (Fig. 7b). Hence, it can be concluded that the geotextile prevents the water migration in

210 the unsaturated soil layer beneath it and helps in the accumulation of moisture above it. A similar
211 observation is reported in various laboratory observations related to one-dimensional flow of water
212 through soil layer in the presence of geotextile (Stormont and Morris, 2000; Bathurst et al., 2009;
213 Zornberg et al., 2010; Bouazza et al., 2013; Azevedo and Zornberg, 2013; Lima et al., 2017).

214 ***3.3 Drainage response of geotextile layer in the presence of vertical gravel drain***

215 In the previous section, the barrier mechanism of the geotextile was observed in the case of the
216 one-dimensional flow of water in unsaturated soil medium, while the lateral flow or the in-plane
217 drainage characteristics of geotextile during rainwater infiltration was not studied thoroughly. The
218 laboratory investigation of horizontal drainage function of geotextile in a soil column is reported
219 in Aristizabal et al. (2016). In this section, the earlier numerical model was modified to study it's
220 the horizontal drainage characteristics of the nonwoven geotextile during rainwater infiltration. A
221 vertical drain composed of Pea gravel was introduced in the numerical model to simulate the facing
222 drain used in different geotechnical infrastructure. The soil water characteristics curve for the
223 drainage layer (Fig. 2) was adopted from Stormont and Anderson (1999). The endpoint of the
224 geotextile was inserted into the vertical drain (Fig. 5c). A toe drain was also inserted at the end
225 point of the vertical drain to provide an escape route for the accumulated water. The boundary
226 conditions and material properties of the model are same as the previous model.

227 After performing the transient seepage analysis, pore water pressure distribution in the soil
228 column is determined and shown in Fig. 6c. The moisture content at the three node points at
229 different time instances is shown in the Fig. 7c. During the infiltration, there is an insignificant
230 change in initial moisture content at Node 3. On the other hand, the moisture content at Node 1
231 and Node 2 gradually increased with the elapsed time. The moisture content at these nodes (1 and
232 2) showed decrement when the geotextile started functioning as horizontal drainage by facilitating

the accumulated water to flow into the vertical drain. Three points (K, L, and M) were chosen at the soil and geotextile interface to see the pore pressure variation with time (Fig. 7d). Point K is above the geotextile within the overlying soil, Point L is on the geotextile and Point M is beneath the geotextile layer within the underlying soil. It can be observed that initially the geotextile functioned as barrier material and water accumulated above the geotextile. As a result, pore water pressure increased above the geotextile layer. Once the suction of the soil above the geotextile reached the breakthrough value, the geotextile functioned as a drainage layer and the pore water pressure above the geotextile layer dissipated (Fig. 7d). It is to be noted that the draining of water through the geotextile layer is a transient phenomenon. Once the water escaped from the geotextile, the pore water pressure above the geotextile dropped below 0 kPa and geotextile became impermeable to the water flow. Further, the process of moisture accumulation over the geotextile layer, the attainment of breakthrough suction and functioning of the geotextile layer as a drainage channel continued alternatively, which can be seen in Fig. 7d. This is further analyzed in the following section considering successive stages of infiltration (wetting and drying cycles). The migration of the water inside the soil column is indicated by water flow vector (Fig. 8). It can be observed that the geotextile acted as a drainage layer and facilitated the water to migrate inside the vertical drain. During this process, water found the easiest way towards more permeable vertical drain instead of entering into the underlying low permeable clay soil. The accumulated water from the geotextile escaped out from the system through the toe drain which is indicated by the water flow vector (Fig. 8). Similar horizontal drainage response of geotextile within an unsaturated soil column is reported in various laboratory studies (Azevedo and Zornberg, 2013; Aristizabal et al., 2016).

3.4 Drainage response of geotextile layer during successive stages of infiltartion

The horizontal drainage characteristics of geotextile were also checked for two successive stages of infiltration (wetting and drying cycles) to observe the hydraulic mechanism occurring through the geotextile. In the first stage, a continuous infiltration was provided for 200 h followed by a zero-infiltration period for 400 h. Further, the second stage of infiltration was carried out for 400 h, which was followed by another zero-infiltration period of 400 h. During the entire duration, the flow characteristics of the soil were monitored. The moisture content and the pore pressure distribution at the three nodes (Node 1, 2 and 3) is shown in Fig. 9. Once the infiltration was stopped at 200 h, the moisture content and pore water pressure at Node 1 and Node 2 decreased, whereas there was no change of moisture content at Node 3. This observation is attributed to the water flowing to the more permeable vertical drain through the geotextile which subsequently escaped out from the toe drain. As soon as the infiltration was stopped at 200 h, the dissipation of accumulated water took place within a short time during the zero-infiltration stage, and porewater pressure less than 0 kPa was attained. There was an insignificant reduction in the volumetric water content and pore water pressure in the zero-infiltration stage after initial dissipation (Fig. 9). The result was attributed to the generation of negative pore water pressure in the soil medium. Hence, the numerical study accentuated that the geotextile functioned as a drainage layer only when the suction of the soil medium was close to 0 kPa (~ air entry value), and the same has been inefficient to expel water in an unsaturated condition of the soil medium beyond air entry suction. The soil suction within the soil column did not revert back to its initial value of 80 kPa, even during successive drying cycles. The aforementioned outcome was achieved due to the capillary effect of the geotextile, which hindered the evaporation of water. Hence, the suction profiles observed on various days indicated that the soil suction remained consistently below 10 kPa.

3.5 Drainage response of geotextile layer due to different initial moisture content of the soil and unsatuarted chracteristics of geotextile

A parametric study was performed to examine the effect of the initial moisture content of the soil on the response of the geotextile. In the previous analysis, the infiltration analysis was performed for the soil column uniformly having initial moisture content 18%. In the current analysis, the initial moisture content of the clay beneath the geotextile layer was considered to be 22%, while maintaining the initial moisture content of the soil above the geotextile as 18%. The idea was to simulate rise of groundwater table during the rainy season which increases the moisture content of the lower soil layer due to capillary rise and identify the drainage response of the geotextile in such circumstance. A transient seepage analysis was conducted for such scenario. The variation of the water content at the three nodes is shown in the Fig. 10. It can be observed that breakthrough occurred to the underlying clay soil due to the increased water content of the soil layer beneath the geotextile. Increase in water content signifies greater hydraulic conductivity of the clay soil, resulting easy migration of water from the geotextile to the underlying soil layer. In the saturated state, geotextile possess greater hydraulic conductivity compared to clay soil. Under the positive pore water pressure condition, geotextile is highly permeable and created a horizontal pathway for the accumulated water to flow towards the vertical drain which is presented by water movement vector diagram (Fig. 10b). From the numerical simulation, it is observed that geotextile functioned as drainage medium once the suction of the interface soil layer reached the breakthrough value. Geotextile is unable to drain water from the system when suction in the soil medium is lesser than the breakthrough suction. Thus, it can be stated that the hydraulic characteristics of the geotextile are effectively simulated in the numerical analysis which may help to understand its drainage function in various soil structure comprising unsaturated marginal soil.

Furthermore, it is imperative to examine the impact of different types of geotextiles on the hydraulic behavior of the soil-geotextile system. The present study examines six distinct categories of geotextiles. Table 2 presents the parameters pertaining to soil water characteristics, whereas Figure 11 depicts the hydraulic properties of the six geotextiles. The original volumetric water content of the soil was determined to be 18%. Figure 12 illustrates the fluctuation in volumetric water content resulting from the implementation of six distinct types of geotextiles for the successive infiltration stages. The geotextile layer has been observed to function as a barrier in all instances, but with varying degrees. The occurrence of barrier breakthrough was not seen for GT-2, GT-5 and GT-6, as their water entry value was found to be relatively low (Fig. 11). In contrast, the water movement was impeded to some degree by GT-1, GT-3, and GT-4 prior to the emergence of the barrier breakthrough mechanism. In the event that the suction at the interface between the soil and geotextile surpasses the air entry value, it is plausible for the geotextile to function as a capillary barrier. Nevertheless, in the event that the suction exerted at the interface between the soil and geotextile was either smaller or equal to the air entry value, the geotextile functioned as a permeable geomaterial, facilitating the passage of water. The aforementioned attribute proved advantageous in facilitating the subsurface drainage of road embankments, soil wall, slopes and necessitates a thorough examination of climatic conditions in order to evaluate drainage function of geotextile in unsaturated soil (Albino et al. 2020). Therefore, based on this data, it can be concluded that the effectiveness of the geotextile's drainage function is substantially determined by its air-entry suction value. This numerical observation is corroborated by the fact that researchers currently working on utilizing wicking geotextile (Lin et al. 2019) with high air entry suction value in the lateral plane direction compared to the cross-plane direction which enable

them to function as horizontal drainage medium in unsaturated state (Lin et al. 2022). However, due to brevity numerical simulation on wicking geotextile is not discussed herein.

4 Conclusions

This work uses numerical simulation techniques to analyze the infiltration characteristics of unsaturated soil medium. The simulation is conducted by calibrating the findings obtained from laboratory tests. The study examines the dual properties (barrier and drainage) of geotextile in an unsaturated soil medium through the examination of transient seepage. The simulation of the drainage characteristics of geotextile was conducted in both the lateral and vertical directions, taking into account the presence or absence of vertical drainage. In addition, an assessment was conducted on the lateral drainage properties of geotextile, taking into account various levels of moisture in the underlying soil and consecutive phases of infiltration, including wetting and drying cycles. A total of seven distinct types of geotextiles are employed in numerical simulations to emphasize the significance of the air entry suction value of geotextiles in relation to their efficacy as lateral drainage systems in unsaturated soil. Based on the conducted analysis, the subsequent results are presented:

- The results of the infiltration simulation conducted on an unsaturated soil column demonstrate that the geotextile effectively acts as a capillary barrier. This barrier prevents the advancement of the saturated wetting front from crossing the geotextile layer and reaching the underlying unsaturated soil until a breakthrough occurs. The capillary barrier phenomenon results in the accumulation of water in the soil above the geotextile layer until the soil's suction near the geotextile reaches the breakthrough threshold.
- The findings of the study indicate that the length of time it takes for a barrier to be breached is notably impacted by both the initial moisture content of the soil surrounding the barrier and

346 the hydraulic characteristics of the geotextile material. The augmentation of water content in
347 the adjacent soil leads to a decrease in the capillary breakthrough time.

348 • Successive stages of infiltration (wetting and drying cycles) indicate insignificant reduction in
349 the volumetric water content and pore water pressure in the zero-infiltration stage (drying
350 cycle) after initial dissipation due to the generation of negative pore water pressure in the soil
351 medium following initial dissipation.

352 • The soil suction within the geotextile reinforced soil column did not revert back to its initial
353 value of 80 kPa, even during successive drying cycles. The aforementioned result was attained
354 as a consequence of the capillary effect exhibited by the geotextile, which impeded the process
355 of water evaporation. Therefore, the suction profiles obtained on different days demonstrated
356 a consistent soil suction level below 10 kPa.

357 • A total of seven distinct types of geotextiles are employed in numerical simulations to
358 emphasize the significance of the air entry suction value of geotextiles in relation to their
359 efficacy as lateral drainage systems in unsaturated soil. Based on the available data, it can be
360 inferred that the efficacy of the geotextile's drainage capability is significantly influenced by
361 its air-entry suction value. The time required to achieve capillary breakthrough is notably
362 diminished when the air entry suction value of the geotextile is increased.

363 • The geotextile functioned as a lateral drainage layer, enabling the movement of water towards
364 the vertical drain. During this procedure, water sought the path of least resistance by infiltrating
365 a more permeable vertical drain rather than permeating the underlying low permeable clay soil.
366 This allowed for the maintenance of a higher suction in the subsurface soil over an extended
367 period of time.

In summary, the numerical study demonstrates the insight of the drainage characteristics of geotextile in unsaturated soil medium which will help the designer to take necessary steps in designing drainage systems considering the unsaturated characteristics of the geotextile.

Data Availability Statement

All the data presented in this study appears in the figures of the manuscript.

Funding

This research did not receive any specific grant from funding agencies in the public, commercial, or not-for-profit sectors.

Conflict of interest statement

The authors declare that there are no conflicts of interest associated with this research.

Author Contribution

AJ: numerical analyses, interpretation of results, and writing—original draft. AD: supervision, and writing—review and editing.

References

AASHTO. 2014. AASHTO LRFD Bridge design specifications. 7th ed. Washington, DC: American Association of State Highway and Transportation Officials.

Albino, U.R., Portelinha, F.H.M. and Futai, M.M., 2020. Numerical simulation of a geotextile soil wall considering soil-atmosphere interaction. Geosynthetics International, 27(4), 394-413.

Aristizabal, E.F.G., Posada, C.A.V., Hernández, A.N.G., 2016. Experimental study of water infiltration on an unsaturated soil-geosynthetic system. Revista Facultad de Ingeniería, Universidad de Antioquia. 78(6), 112-118.

Azevedo, M., Zornberg, J. G., 2013. Capillary barrier dissipation by new wicking geotextile. In *Advances in Unsaturated Soils - Proceedings of the 1st Pan-American Conference on Unsaturated Soils, PanAmUNSAT 2013,* 559-565.

Bathurst, R.J., Siemens, G., Ho, A.F., 2009. Experimental investigation of infiltration ponding in one-dimensional sand-geotextile columns. Geosynthetics International. 16(3), 158-172.

Benjamim, C.V., Bueno, B., Zornberg, J.G., 2007. Field monitoring evaluation of geotextile-reinforced soil retaining wall. Geosynthetics International. 14 (2), 100-118.

Bhattacherjee, D., Viswanadham, B.V.S., 2015. Numerical studies on the performance of hybrid-geosynthetic-reinforced soil slopes subjected to rainfall. Geosynthetics International. 22(6), 411-427.

Biswas, N., Puppala, A.J., Khan, M.A., Congress, S.S.C., Banerjee, A. and Chakraborty, S., 2021. Evaluating the performance of wicking geotextile in providing drainage for flexible pavements built over expansive soils. Transportation Research Record, 2675(9), 208-221.

405 Bouazza, A., Zornberg, J.G., McCartney, J.S., Nahlawi, H., 2006. Significance of unsaturated
406 behavior of geotextiles in earthen structures. Australian Geomechanics. 41(3), 133-142.

407 Bouazza, A., Zornberg, J.G., McCartney, J.S., Singh, R.M., (2013) Unsaturated geotechnics
408 applied to geoenvironmental engineering problems involving geosynthetics. Engineering
409 Geology. 165(1), 143-153

410 Christopher, B.R., Stuglis, R.S., 2005. Low permeable backfill soils in geosynthetic
411 reinforced soil wall: state of the practice in North America: state of the practice
412 in North America. Proceedings of North American Geo-synthetics Conference
413 (NAGS 2005), Las Vegas, Nevada, USA, GRI-19, pp. 1-16.

414 Esmaili, D., Hatami, K., Miller, G.A., 2014. Influence of matric suction on geotextile
415 reinforcement marginal soil interface strength. Geotextiles and Geomembranes. 42(2), 139–
416 53.

417 GeoStudio Manual, 2012. Seepage Modeling with SEEP/W. Geo-Slope International Ltd, Alberta

418 Iryo, T., Rowe, R. K., 2004. Numerical study of infiltration into a soilgeotextile column.
419 Geosynthetics International. 11(5), 377-389.

420 Iryo, T., Rowe, R.K., 2003. On the hydraulic behaviour of unsaturated nonwoven geotextiles.
421 Geotextiles and Geomembranes. 21(6), 381-404.

422 Iryo, T., Rowe, R.K., 2005. Infiltration into an embankment reinforced by nonwoven geotextiles.
423 Canadian Geotechnical Journal. 42(4), 1145-1159.

Jana, A., Dey, A., 2016. Effectiveness of Geotextile Reinforced Soil Walls Backfilled with Fine Soil. 6th Asian Regional Conference on Geosynthetics- Geosynthetics for Infrastructure Development, New Delhi, India, 440-449.

Jana, A., Dey, A., 2017. Combined Functioning of Geotextile as Barrier and Drainage Material in Unsaturated Earth Retaining Structures. Indian Geotechnical Journal, 1-18.

Kim, S.K., Borden, R.H., 2013. Numerical simulation of MSE wall behavior induced by surface-water infiltration. Journal of Geotechnical and Geoenvironmental Engineering, ASCE. 139(12), 110–124.

Lima M.J., Azevedo M.M., Zornberg J.G., Palmeira, E.M., 2018. Capillary barriers incorporating non-woven geotextiles. Environmental Geotechnics. 5(3), 1-8.

Lin, C., Zhang, X. and Han, J., 2019. Comprehensive material characterizations of pavement structure installed with wicking fabrics. Journal of Materials in Civil Engineering, 31(2), p.04018372.

Lin, C., Zhang, X., Galinmoghadam, J., and Guo, Y. 2022. Working mechanism of a new wicking geotextile in roadway applications: A numerical study. Geotextiles and Geomembranes, 50(2), 323-336.

Mitchell, J.K., Zornberg, J.G., 1995. Reinforced soil structures with poorly draining backfills, Part II: Case histories and applications. Geosynthetics International. 2(1), 265-307.

Miyata, Y., Bathurst, R.J., 2007. Development of K-stiffness method for geosynthetic reinforced soil walls constructed with c-φ soils. Canadian Geotechnical Journal. 44(12), 1391–1416.

444 NCMA, 201. Design manual for segmental retaining walls. 3rd ed. National Concrete Masonry
445 Association.

446 Portelinha, F.H.M., Bueno, B.S., Zornberg J.G., 2013. Performance of nonwoven geotextile
447 reinforced soil walls under wetting conditions: Laboratory and field investigation.
448 Geosynthetics International. 20(2), 90-104.

449 Portelinha, F.H.M., Zornberg, J.G., 2017. Effect of infiltration on the performance of an
450 unsaturated geotextile-reinforced soil wall. Geotextiles and Geomembranes. 45(3), 211-226.

451 Portelinha, F.H.M., Zornberg, J.G., Pimentel, V., 2014. Field performance of retaining walls
452 reinforced with woven and nonwoven geotextiles. Geosynthetics International. 21(4), 270-284.

453 Richards, L.A., 1931. Capillary conduction of liquids through porous mediums. Journal of Applied
454 Physics. 1, 318–333.

455 Stormont, J.C., Anderson, C.E., 1999. Capillary barrier effect from underlying coarser soil layer.
456 Journal of Geotechnical and Geoenvironmental Engineering, ASCE. 125, 641-648.

457 Stormont, J.C., Morris, C.E., 2000. Characterization of unsaturated nonwoven geotextiles.
458 Proceedings of Advances in Unsaturated Geotechnics, GeoDenver 2000. 529–542.

459 Tatsuoka, F., Yamauchi, H., 1986. A reinforcing method for step clay using a non-woven
460 geotextile. Geotextiles and Geomembranes. 4, 241-268.

461 Thuo, J.N., Yang, K.H., Huang, C.C., 2015. Infiltration into unsaturated
462 reinforced slopes with nonwoven geotextile drains sandwiched in sand layers.
463 Geosynthetics International. 22(6), 457-474.

Vahedifard, F., Mortezaei, K., Leshchinsky, A.B., Leshchinsky, D., Lu, N., 2016. Role of suction stress on service state behavior of geosynthetic-reinforced soil structures. Transportation Geotechnics. 8, 45-56.

van Genuchten, M.Th., 1980. A closed-form equation for predicting the hydraulic conductivity of unsaturated soils. Soil Science Society of America. 44, 892-898.

Zornberg, J.G., Azevedo, M.M., Pickles, C.B., 2017. Evaluation of the Development of Capillary Barriers at the Interface between Fine-grained Soils and Nonwoven Geotextiles. Geotechnical Special Publication (GSP) 275, Geosynthetics, Forging a Path to Bona Fide Engineering Materials, ASCE, Proceedings of the GeoChicago 2016 Conference, Chicago, IL. 159-167.

Zornberg, J.G., Bouazza, A., McCartney, J.S., 2010. Geosynthetic capillary barriers: Current state of knowledge. Geosynthetics International. 17(5), 273-300.

List of Tables

Table 1 Hydraulic parameters of soil and geotextile for cylindrical soil column test

Material	a (1/kPa)	n	Saturated water content θ_s	Residual water content θ_r	Saturated hydraulic conductivity (m/hr)	References
Clay	0.21	1.5	0.46	0.05	4.32×10^{-3}	Bouazza et al., 2006
Sand	0.56	4.8	0.38	0..3	1.908	Bouazza et al., 2006
Geotextile	1.569	7	0.99	0.02	6.84	Bouazza et al., 2006
Gravel	33.33	2.5	0.33	0.03	46.8	Stormont and Anderson, 1999

Table 2 **Hydraulic parameters geotextiles for sensitivity analysis**

Geotextile	a (1/kPa)	n	Saturated water content θ_s	Residual water content θ_r	Saturated hydraulic conductivity (m/h)	References
GT-1	2.577	1.68	0.754	0	12.384	Stormont and Morris, 2000
GT-2	3.891	6.9	0.6	0	23.76	Stormont and Ramos, 2004
GT-3	11.10	2.5	0.86	0.1	5.22	Iryo and Rowe, 2003
GT-4	8.46	4.95	0.821	0.07	82.8	Zornberg et al., 2017
GT-5	3.0	3.0	0.92	0	6.012	Iryo and Rowe, 2005
GT-6	5.0	7	0.24	0	108	McCartney and Zornberg J.G., 2010; Thuo et al (2015)

List of Figures

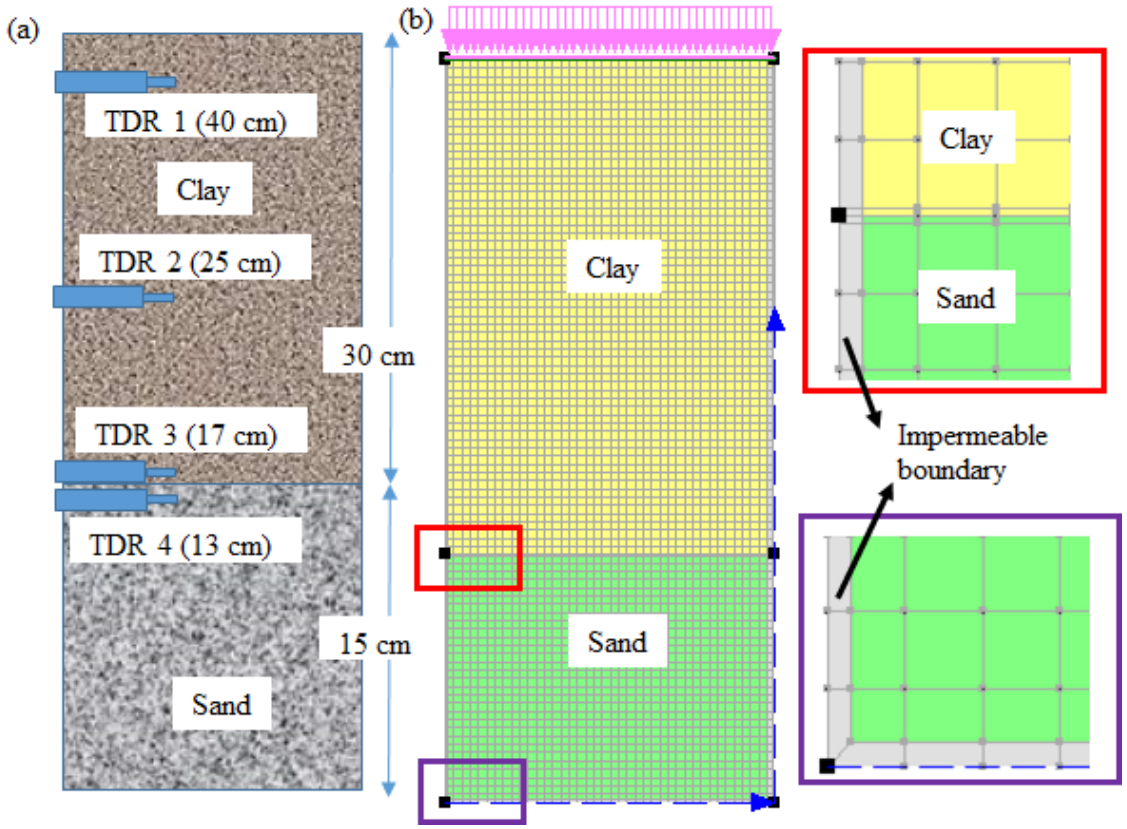

Figure 1. (a) Schematic representation of cylindrical soil column (Modified after Bouazza et al., 2006, 2013) (b) One-dimensional finite element model of the soil column

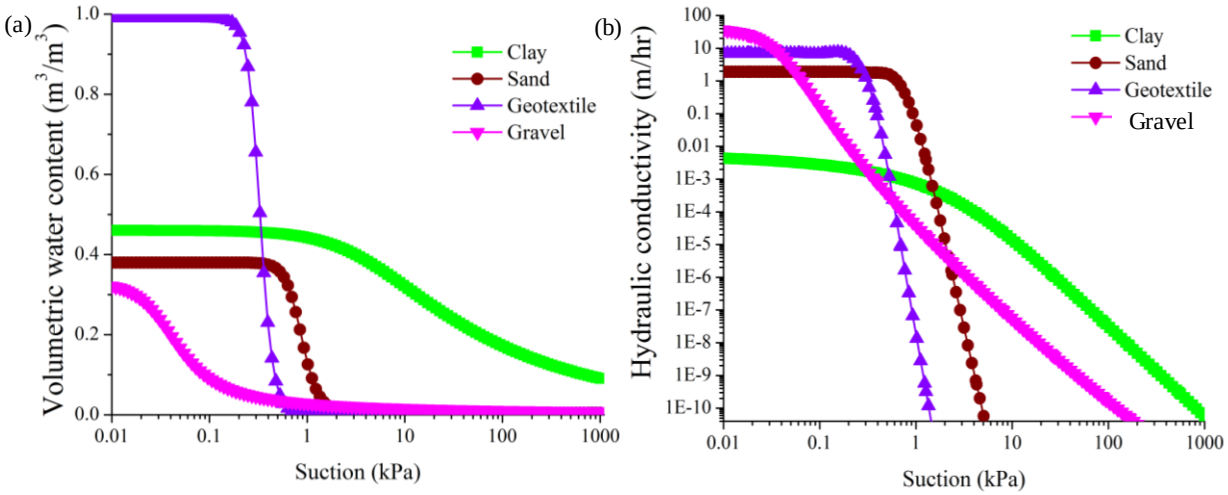

Figure 2. Hydraulic characteristics of soil and geotextile used in cylindrical soil column test (a) Water retention curves (b) Hydraulic conductivity curves

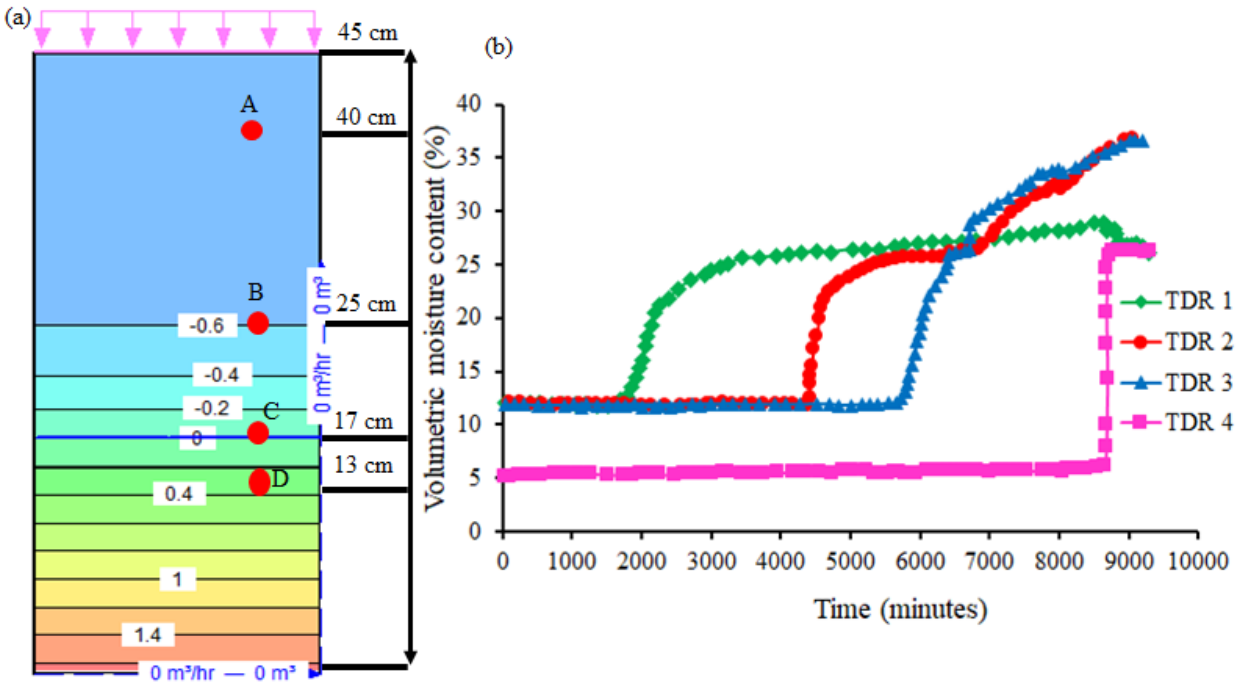

Figure 3. (a) Pore water pressure profiles (in kPa) from numerical simulations (b) Experiment results showing volumetric water content with depth in the cylindrical soil column (Modified after Bouazza et al. 2006, 2013)

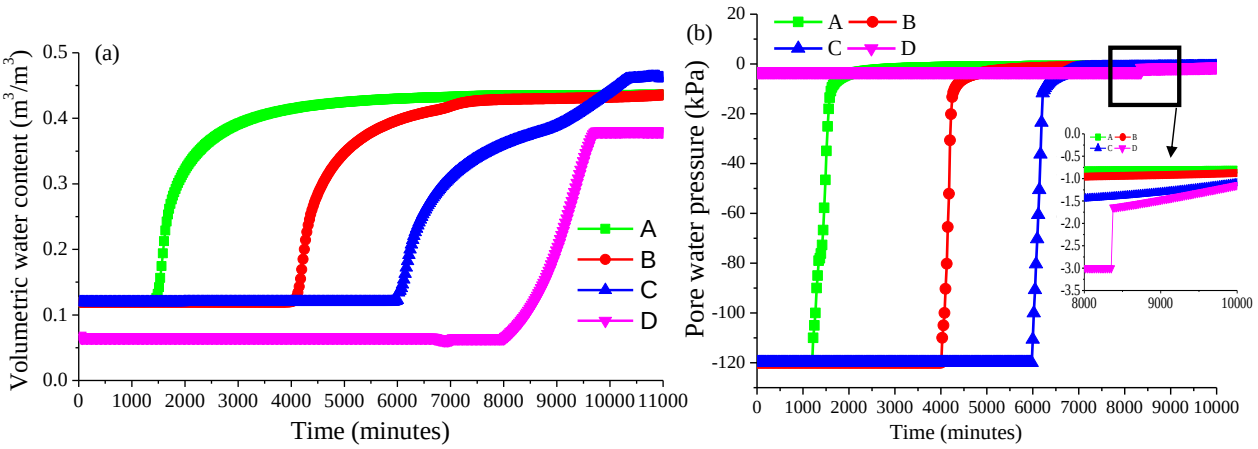

513

514 **Figure 4. Numerical simulation results of infiltration in the soil column (a) volumetric**
515 **water content (b) pore water pressure distribution with time**

516

517

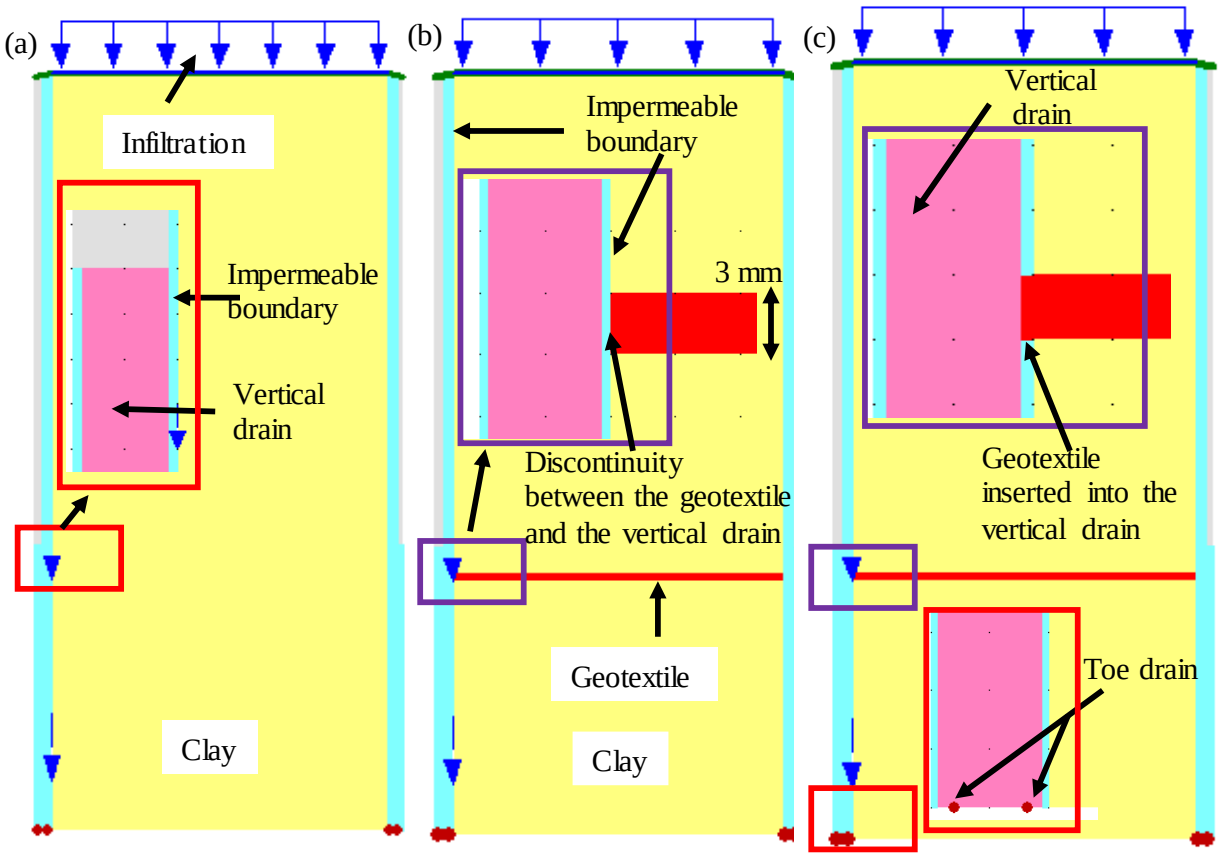

518

519 **Figure 5. Numerical models of the soil column infiltration tests: (a) soil column without**
520 **geotextile (b) soil column with a geotextile layer located at a depth of 30 cm (c) soil column**
521 **with the same geotextile layer inserted into the vertical gravel drain**

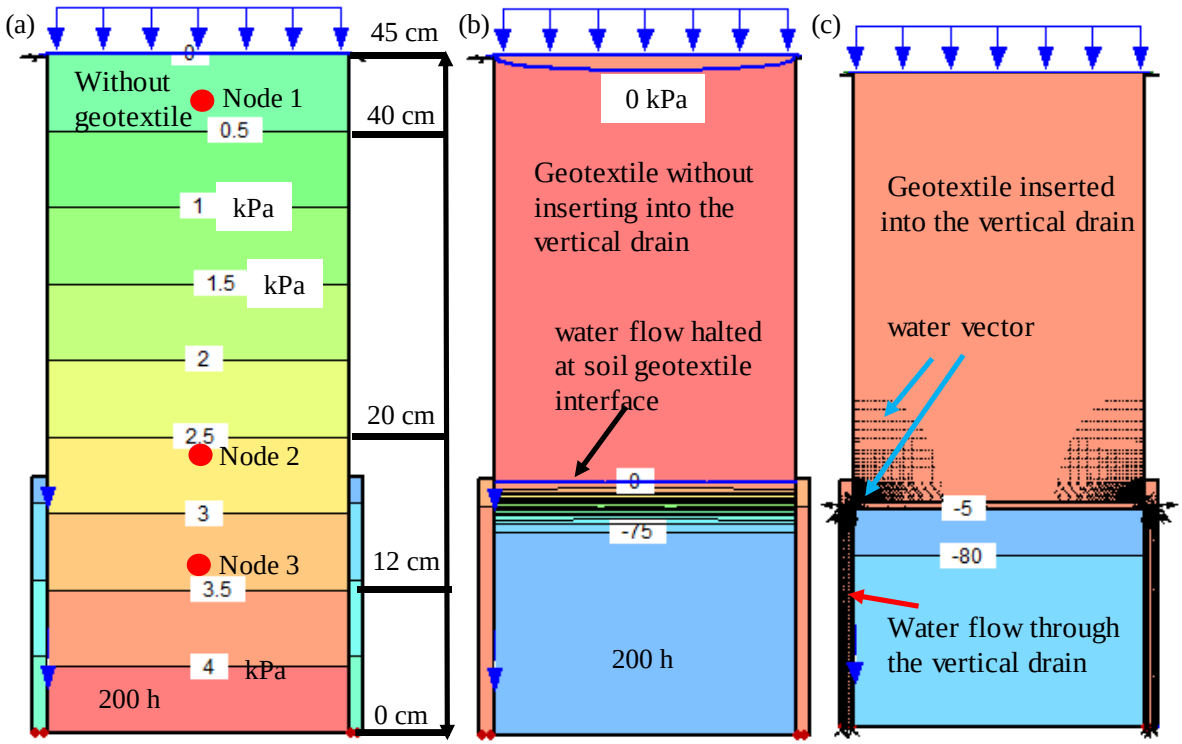

Figure 6. Numerical simulation results showing pore water pressure distribution (a) soil column without geotextile (b) soil column with geotextile layer (c) soil column with geotextile layer inserted into the vertical gravel drain

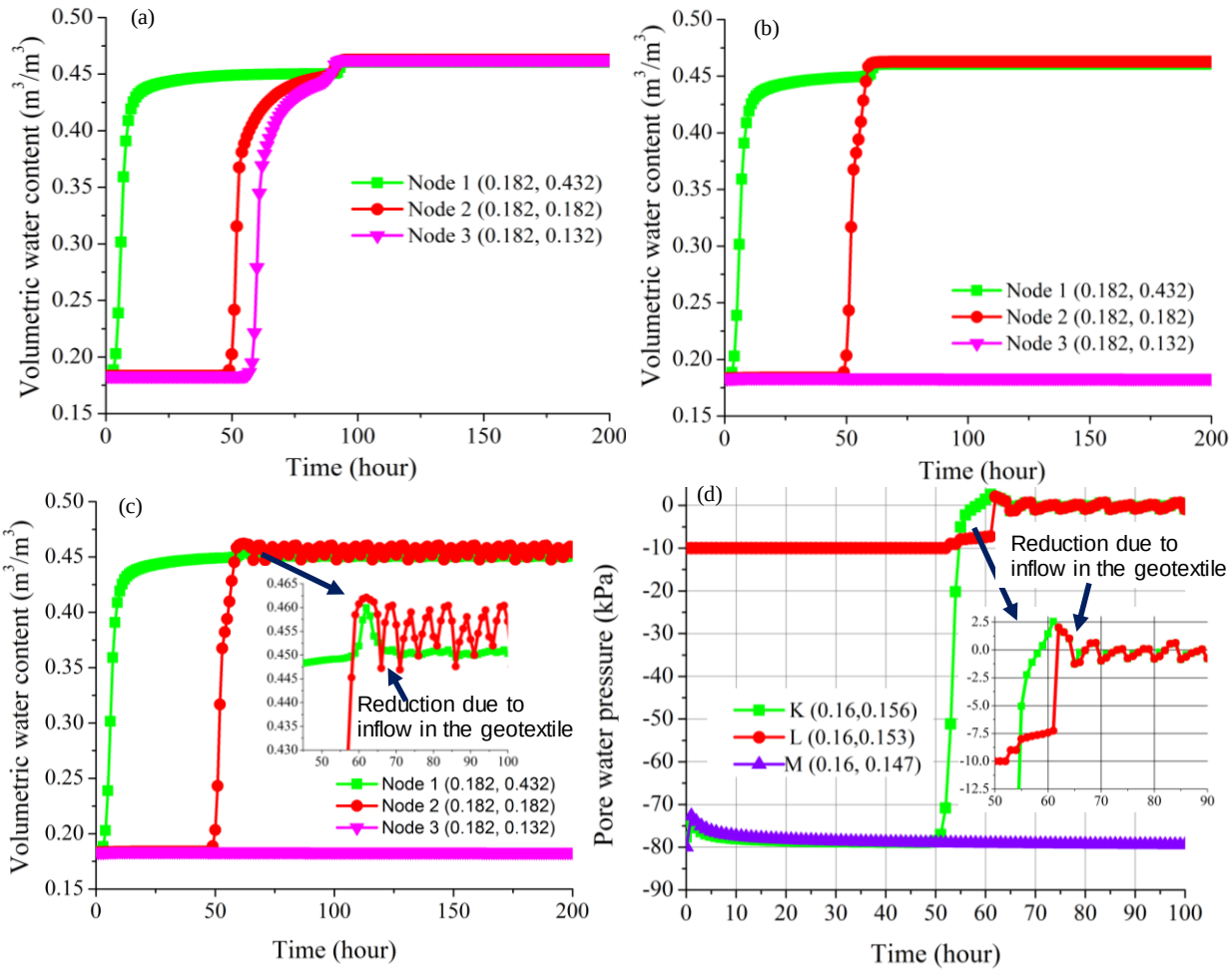

526

527 **Figure 7. Variation of volumetric water content with time at the selected time history**
528 **nodes (a) without geotextile layer (b) with geotextile layer (c) with geotextile layer inserted**
529 **into the vertical gravel drain (d) Variation of pore water pressure at soil geotextile**
530 **interface for the case of geotextile layer inserted into the vertical gravel drain**

531

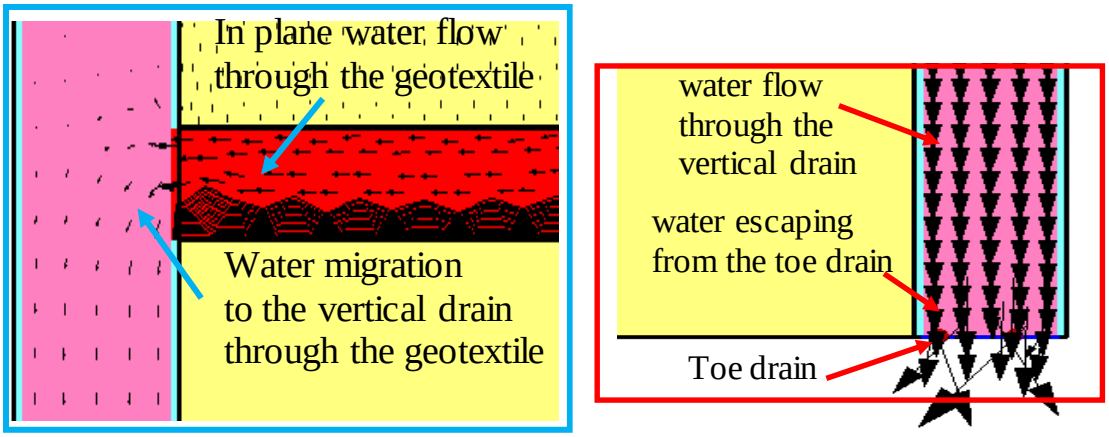

Figure 8. Water flow vector through the soil column showing in plane drainage function of geotextile

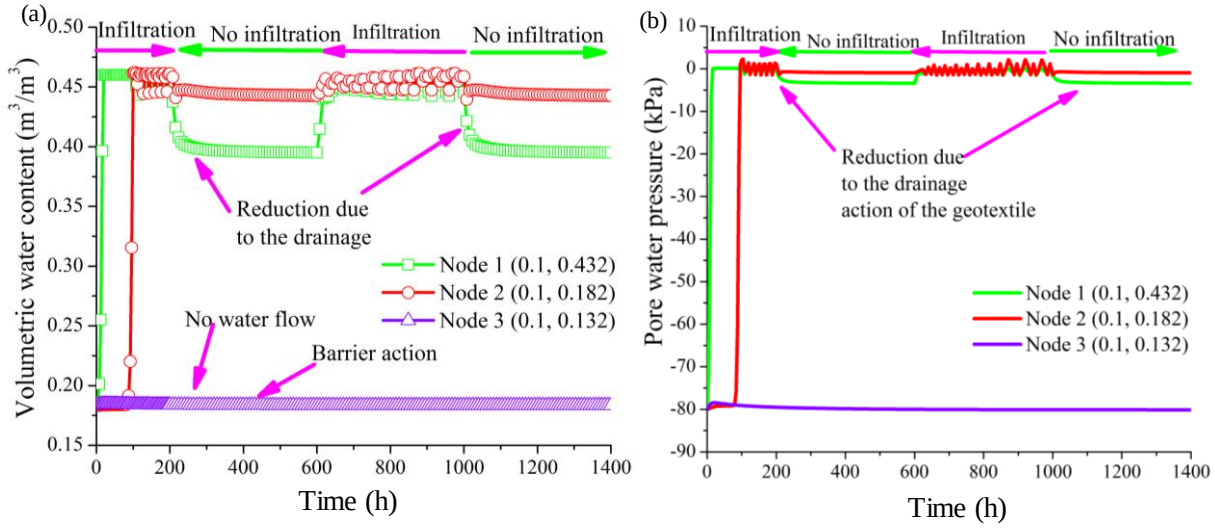

Figure 9. Drainage characteristics of geotextile at different infiltration period showing (a) volumetric water content (b) pore water pressure variation at three-time history points

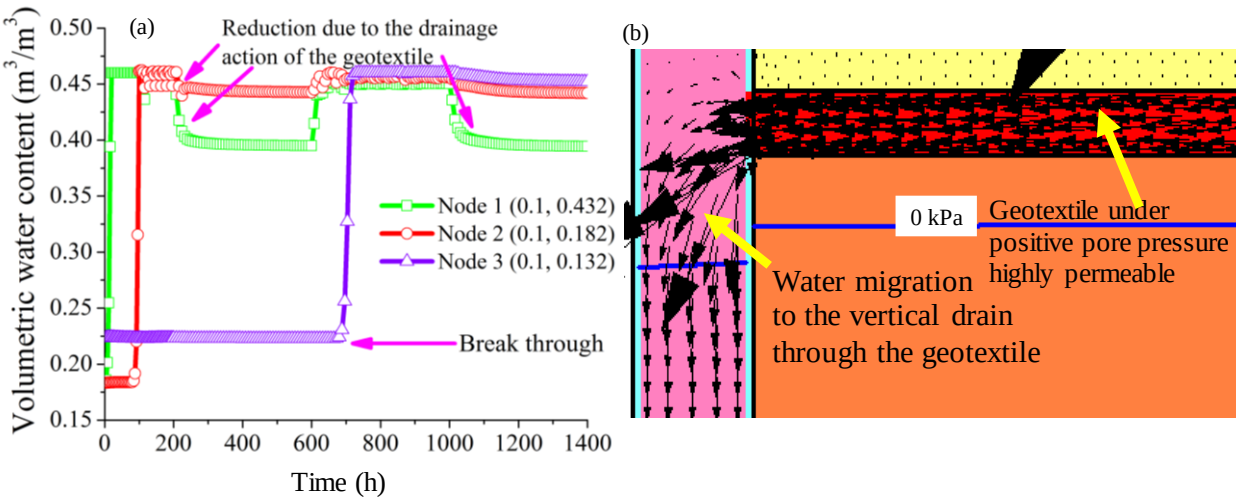

556

557 **Figure 10. Barrier breakthrough of the geotextile layer due to increase in initial**
558 **moisture content of the soil layer beneath the geotextile layer (b) Water flow vector**
559 **through the geotextile under saturated condition after barrier breakthrough**

560

561

562

563

564

565

566

567

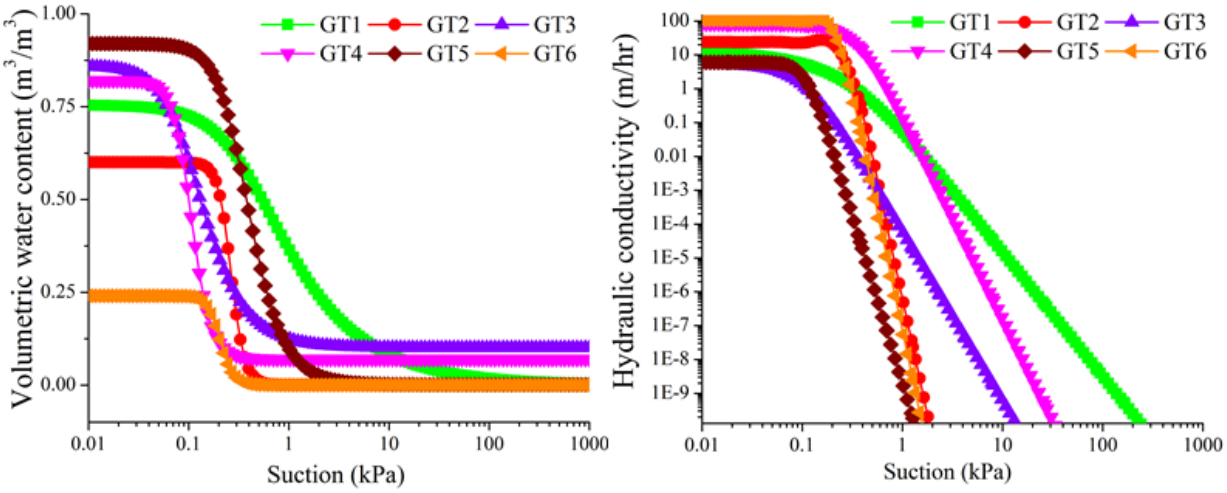

568

569 **Figure 11. Hydraulic properties of different geotextiles used in the present study: a**

570 **water retention curves b hydraulic conductivity curve**

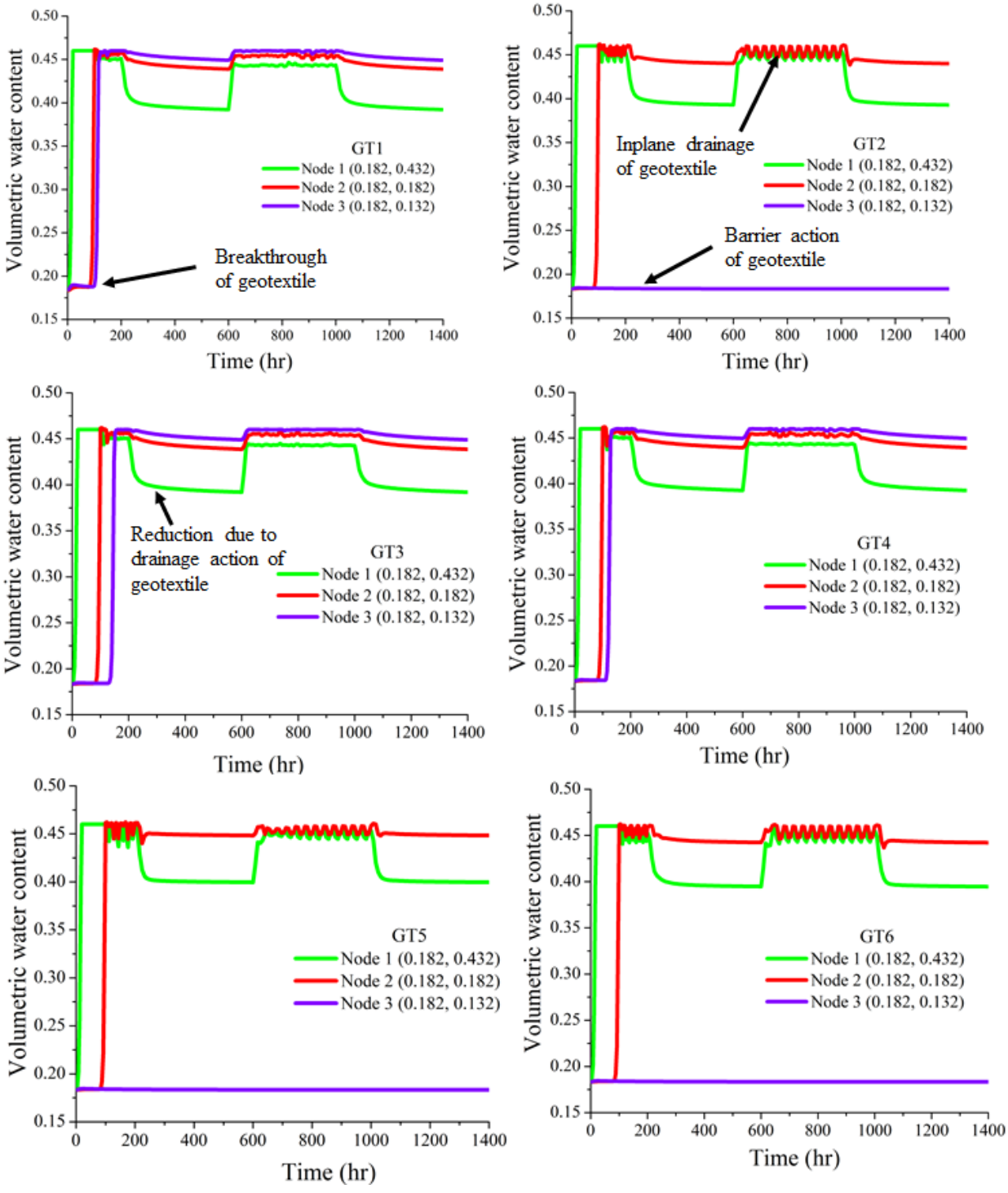

Figure 12. The effect of utilizing different geotextiles on the volumetric water content of the model soil columns